Suction of hydrosoluble polymers into nanopores

Lucie Béguin, Bruno Grassl, Françoise Brochard-Wyart, Mohammed Rakib, Hervé Duval

Soft Matter

Dynamic Article Links

Cite this: *Soft Matter*, 2011, **7**, 96

www.softmatter.org

PAPER

Suction of hydrosoluble polymers into nanopores

Lucie Béguin,[a] Bruno Grassl,[b] Françoise Brochard-Wyart,[c] Mohammed Rakib[a] and Hervé Duval*[a]

Received 27th May 2010, Accepted 2nd August 2010
DOI: 10.1039/c0sm00443j

Forced penetration of large hydrosoluble polymer chains through track-etched membranes has been investigated as a function of both solvent flow rate in the pores and the ratio of polymer hydrodynamic radius to pore radius. We measure the rejection coefficient R_{obs} from retentate and permeate mean concentrations, and its corrected value R including polymer accumulation at the membrane. The variations of R as a function of solvent flow rate per pore in adimensional units collapse into the same curve well fitted by de Gennes' "suction model". This curve, universal for flexible polymers in good solvents, leads to an estimate of the critical penetration flow.

1. Introduction

The transport of flexible polymers in solution through porous media controls many processes: size exclusion chromatography, ultrafiltration and enhanced oil recovery (extraction of oil from porous geological structures by injection of a high molecular weight polymer solution).

A simple view of the passage of polymers through porous media is purely geometrical: solutes of a size comparable to or larger than the pore size cannot easily penetrate.

This picture is relevant for polymer solutions in the dilute regime when the solutions are immobile or when the solvent flow is low. However, flexible polymers deviate from hard-sphere behaviour and penetrate small pores when the polymer concentration or the solvent flow rate is increased.[1]

Using the scaling approach,[2] Daoudi and Brochard[3] have evaluated the static partition coefficient (*i.e.*, the ratio of the solute concentration inside the pore to the solute concentration outside) of polymer chains in a good solvent, in both dilute and semi-dilute regimes. Daoudi and Brochard's predictions have been qualitatively confirmed in several experimental studies.[4–6] Guillot *et al.*[7] could handle quantitative validations by studying the diffusion of polymer chains through a track-etched membrane with cylindrical pores. In the dilute regime, the parameter that controls the passage of the chains is the ratio λ of the hydrodynamic radius r_h to the pore radius r_p: for $\lambda > 1$, the chains are excluded. When the concentration is increased in the semi-dilute regime, the relevant parameter is the average distance between entanglements which represents the screening length for both excluded volume and hydrodynamic interactions: in the semi-dilute regime, chains penetrate pores up to a diameter of the order of the screening length.

Furthermore, Daoudi and Brochard[3] have studied the penetration of polymer chains into pores driven by hydrodynamic flows in the case of a good solvent. They propose the "affine stretching model". The broad lines of their model are the following: as the flow of solvent is convergent at the entrance of the pores, the velocity field is assumed to be:

$$v(r) \approx \frac{q_p}{r^2} \tag{1}$$

where r is the distance from the pore and q_p is the flow in one pore. It leads to an elongational shear:

$$s(r) = -\frac{dv}{dr} \approx \frac{q_p}{r^3} \tag{2}$$

An isolated molecule subjected to an elongational flow is slightly deformed if the elongational shear s is less than a critical value s_c. On the contrary, the molecule follows the deformation imposed by the solvent if $s \geq s_c$. This type of deformation is called "affine", meaning that the molecule is deformed in the same way as a fluid element. The critical shear value is of the order of the Zimm relaxation frequency of the polymer chain:

$$s(r) \approx \tau_Z^{-1} \approx \frac{k_B T}{\eta_s r_g^3} \tag{3}$$

where k_B is the Boltzmann constant, T is the temperature of the solution, η_s is the solvent dynamic viscosity and r_g is the gyration radius of the polymer. If r_c is the distance at which $s = s_c$, the chain is stretched at a distance $r \leq r_c$ from the pore and its affine transverse deformation (the longitudinal direction coincides with the pore axis) is

$$R_\perp(r) = r_g\left(\frac{r}{r_c}\right) \tag{4}$$

The entrance condition $R_\perp(r_p) = r_p$ leads to $r_c = r_g$. Thus, the critical solvent flow rate for a chain to enter into a pore is given by:

[a]*Ecole Centrale Paris, Laboratoire de Génie des Procédés et Matériaux, Grande Voie des Vignes, 92295 Châtenay-Malabry Cedex, France*
[b]*Université de Pau et des Pays de l'Adour, IPREM UMR CNRS/UPPA 5254, Hélioparc Pau Pyrénées, 2 Avenue du Président Angot, 64053 Pau cedex 09, France*
[c]*Institut Curie, Laboratoire PCC/UMR 168, 11 rue Pierre et Marie Curie, 75231 Paris Cedex 05, France*

$$q_p^c \approx \frac{k_B T}{\eta_s} \quad (5)$$

q_p^c is surprisingly independent of both molecular size and pore radius. Furthermore, the Daoudi and Brochard model predicts a sharp transition from full retention to forced penetration at the critical flow rate.

Experimental evidence of forced penetration is reported in the literature for the following polymers in good solvent: PEG (molecular weight 1.5×10^4–3.5×10^4 Da, λ unknown) in water,[5] dextran (7×10^4–2×10^6 Da, λ unknown) in water,[5] polystyrene (10^5–2×10^7 Da, $\lambda = 0.8$–4.1) in a mixed solvent of 90% tetrachloride–10% methanol,[8] polystyrene (7.75×10^5–6.8×10^6 Da, $\lambda = 0.8$–1.2, 10^5–3.5×10^5 Da, λ unknown) in ethyl acetate,[9,10] polystyrene (3.5×10^4 Da and 6.9×10^6 Da, $\lambda = 0.9$ and 9.9) in toluene.[11]

These experiments have been essentially performed in pressure driven dead-end ultrafiltration devices and basically consist of measuring the observed rejection coefficient, R_{obs}, of the polymer, *i.e.*,

$$R_{obs} = 1 - \frac{c_p}{c_r} \quad (6)$$

where c_p and c_r are the polymer concentration in the permeate (low pressure side) and in the retentate (high pressure side), respectively. Usually,[5,8,10] the solution in the high pressure side of the ultrafiltration device is mechanically agitated in order to reduce boundary layer effects (*i.e.*,"concentration polarisation"). In that very case, the solute concentration c_m at the membrane surface tends to the bulk solution concentration c_r and, consequently, the observed rejection coefficient can be assimilated to the true rejection coefficient defined by

$$R = 1 - \frac{c_p}{c_m} \quad (7)$$

R is closely related to the partition coefficient of the polymer between the inside and outside of the pores and is the relevant quantity for analysing the suction of the polymer chains.

Some authors[8,9,11] use well-controlled systems, as required for quantitative results, consisting of mono-disperse flexible polymers and well-calibrated membranes such as track-etched ones. Hence, Long and Anderson[8] performed ultrafiltration of polystyrene solutions through track-etched mica sheets in an agitated cell. They observed that the true rejection coefficient is independent of polymer and pore dimensions (as long as $r_h > r_p$) and is only a function of solvent flow rate per pore, a result consistent with scaling law predictions.[3]

However, most studies[5,8–10] report a smooth transition from total retention to forced penetration, except for Jin and Wu,[11] who observed a sharp transition at a critical solvent flow rate. To intercept a smooth transition, de Gennes[12] constructed the "suction model", which gives rise to an energy barrier to enter the pore, and a spreading of the transition.

More recently, Markesteijn *et al.*[13] performed mesoscale simulations to investigate forced penetration of polymers into nanopores. Their numerical results confirm that the critical solvent flow rate is independent on λ, depends linearly on the temperature and is inversely proportional to solvent viscosity. Moreover, their numerical results show a smooth transition from total retention to full transmission.

In order to experimentally study and characterise the transition from total retention to forced penetration, we have undertaken a series of experiments using a high molecular weight hydrosoluble polymer, track-etched membranes and a cross-flow ultrafiltration set-up. Special care has been taken to analyse the molecular weight distribution of the polymer and to characterise the membrane microgeometry. The polarisation effects that control polymer concentration at the membrane surface have been carefully included.

In the present paper, we measure the permeate flow and the observed rejection coefficient of the polymer for different values of the transmembrane pressure and of the polymer concentration. Then, we derive the true rejection coefficient using a model for the polymer accumulation at the membrane. We analyse its variations with the solvent flow rate per pore, using de Gennes' "suction model".[12] Finally, we give an experimental estimate of the critical solvent flow rate per pore leading to polymer suction.

2. Experimental methods

2.1. Membranes

We used commercialised track-etched polycarbonate membranes coated with polyvinylpyrrolidone. These membranes, supplied by GE Osmonics, are symmetric and have controlled cylindrical pores. The experiments were performed on membrane models KN3CP81030 and KN5CP81030. These models essentially differ by their nominal pore diameter, equal to 30 nm and 50 nm, respectively, as given by the supplier. They are referred to below as TEM_0.03 and TEM_0.05, respectively.

Two techniques were used to characterise the membrane microgeometry; they are discussed below.

(a) Scanning electron microscopy (SEM). The membranes were observed with a field emission scanning electron microscope (LEO 1530) after deposition of a 5 nm thick tungsten film (using a PECS, Precision Etching Coating System, from Gatan). The micrographs (5 per membrane model) were analysed and processed using the public domain software ImageJ in order to determine pore size distribution and the mean pore density of the membrane models.[14] Fig. 1 presents the cumulative pore size distributions of TEM_0.03 (measured mean pore radius $r_p^0 = 23$ nm, mean standard deviation $\sigma = 4$ nm) and TEM_0.05 ($r_p^0 = 35$ nm, $\sigma = 5$ nm). It should be noted that the measured mean pore diameter is greater than the nominal pore diameter given by the supplier. The mean pore density is equal to $n_p = 7.2 \pm 0.2 \times 10^{12}$ pores m^{-2} and $n_p = 6.5 \pm 0.2 \times 10^{12}$ pores m^{-2}, for TEM_0.03 and TEM_0.05, respectively, in good agreement with the GE Osmonics specifications, *i.e.* 6×10^{12} pores m^{-2} $\pm$ 15% for both membrane models. The thickness of both membrane models is equal to $l = 6.5 \pm 0.4$ μm (GE Osmonics specification, 6 μm $\pm$ 10%).

(b) Pure solvent permeability. The hydraulic resistance R_m of the membranes is systematically determined by measuring the flux J_v of milliQ water (conductivity 18 MΩ and TOC < 3 ppb) through the membranes under constant pressure head (TMP = 0.2–2 bars, by 0.2 bar pressure increment). The measured hydraulic resistances ($R_m = 5.1 \pm 0.5\ 10^{12}$ m^{-1} and $R_m = 1.4 \pm 0.1$

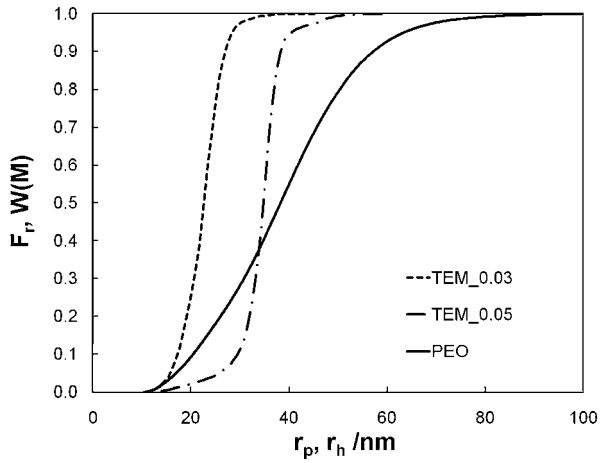

Fig. 1 Cumulative pore size distribution (F_r) of membrane models TEM_0.03 (dash line) and TEM_0.05 (dash-dot line) against the pore radius (r_p) and cumulative molar mass distribution ($W(M)$) of PEO (solid line) against the hydrodynamic radius (r_h).

10^{12} m^{-1} for TEM_0.03 and TEM_0.05, respectively) are slightly lower than the hydraulic resistance calculated from the mean pore distribution and mean pore density assuming Poiseuille flow in the pores ($R_m = 6.6 \times 10^{12}$ m^{-1} and $R_m = 1.5 \times 10^{12}$ m^{-1}, respectively). This discrepancy, which increases as the pore mean diameter decreases, has already been mentioned in the literature[15] and is attributed to the real form of the pores, which are more like cigars than straight cylinders. It should be noted that as the discrepancy in R_m is equal to 25% and 5% for TEM_0.03 and TEM_0.05, respectively, and as the hydraulic resistance roughly scales as $R_m \sim (r_p^0)^{-4}$, we expect the pore radius to vary slightly along the pore axis.

2.2. Polymer solution

The hydrosoluble polymer used is a large molar mass polyethylene oxide (PEO) supplied by Sigma Aldrich (CAS number 25322-68-3, nominal molar weight equal to 10^6 g mol^{-1}). The polymer, in powder form, is dissolved in milliQ water at concentrations ranging from 0.05 g L^{-1} to 0.3 g L^{-1}. Solutions are homogenized by gentle magnetic agitation for 9 h.

The PEO concentration of the permeates and retentates resulting from ultrafiltration is measured by differential refractometry (Knauer Differential Refractometer). Uncertainty of concentration measurement is below 2%.

The weight-average molar mass (M_w), radius of gyration (r_g), polydispersity (I_p), and differential molar mass distribution ($w(M)$) of the PEO samples were determined by size exclusion chromatography (SEC) using a Waters Alliance 2690 (USA) chromatograph equipped with three Shodex OHpak columns (SB-806HQ, SB-804HQ, and SB-802.5HQ) and two online detectors: a differential refractometer and a Dawn DSP light scattering detector (MALS) from Wyatt (USA) equipped with a K5 cell and a He–Ne laser ($\lambda = 632.8$ nm). A 0.1 M solution of $NaNO_3$ was used as the eluent at a flow rate of 0.5 mL/min. Samples were prepared by dissolving the polymers in 0.1 M $NaNO_3$ and then filtering with a 0.45 μm filter (Millipore) after about 24 h. 100 μL of the solutions were injected at a concentration of about 0.2 mg/mL. The weight-average molar mass, radius of gyration, and polydispersity were obtained from data collected and analysed using ASTRA SEC-software (version 4.90, Wyatt Technology Corp., USA). The calculations of molar mass and radius of gyration were carried out according to the Zimm fit method ($dn/dc = 0.135 \pm 0.002$ mL/g in 0.1 M $NaNO_3$).[16] Systematic errors occur because of incorrect values of dn/dc, refractometer calibration factor k and the band-broadening effect. The band-broadening correction was not considered because this correction did not affect the final results. The effects of k and dn/dc on the weight-average molar mass M_w are proportional to k^{-1} and $(dn/dc)^{-1}$, respectively (no effect on r_g). For the M_w value, this systematic error can be prevented by using the same refractometer detector for the k and dn/dc determinations. The error limit is estimated at 8% on M_w and r_g, based on the mean standard deviation from multiple injections.[17]

The differential molar mass distribution of the PEO before ultrafiltration is reported in Fig. 2. Its weight-average molar mass is equal to $M_w = 1.1 \times 10^6$ g mol^{-1} and its polydispersity to $I_p = 1.61$. Its z-average gyration radius is equal to $r_g = 84.5$ nm. The values of r_g are correctly described by the scaling law $r_g \sim M_w^{0.61}$: it can be observed that the value of the Flory exponent is characteristic of a good solvent system and in accordance with the value obtained by Devanand and Selser,[18] *i.e.* $r_g \sim M_w^{0.58 \pm 0.03}$, for PEO with molar mass from 10^5 to 10^6 g mol^{-1}. Knowing the differential molar mass distribution of the PEO before ultrafiltration and using the relation between the hydrodynamic radius r_h and M_w established for PEO by Devanand and Selser,[18] *i.e.* $r_h = 1.45 \times 10^{-2}\ M_w^{0.57 \pm 0.01}$ nm, we could determine the weight-average hydrodynamic radius of the PEO, *i.e.* $r_h = 41.4$ nm. It is also deduced (see Fig. 1) that the mass fraction of PEO with a hydrodynamic radius greater than $r_p^0 = 23$ nm (resp. $r_p^0 = 35$ nm), *i.e.* the average radius of TEM_0.03 pores (resp. TEM_0.05), is equal to 86% (resp. 61%). Finally the average steric hindrance of PEO characterised by the ratio $\lambda = r_h/r_p^0$ is equal to 1.2 and 1.8 for TEM_0.03 and TEM_0.05, respectively.

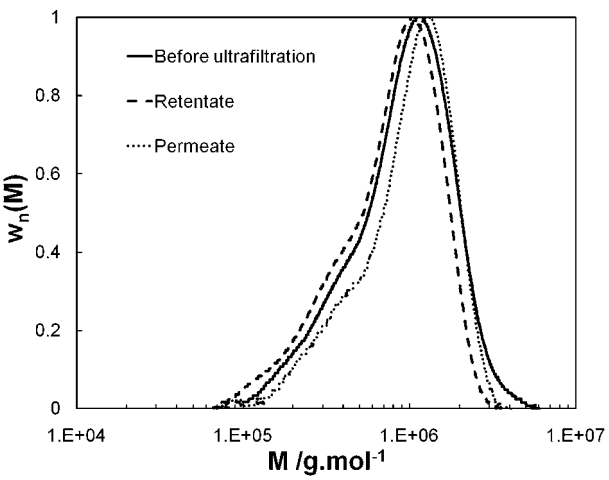

Fig. 2 Normalized differential molar mass distribution of the PEO ($w_n(M)$) as a function of the molar mass (M). Before ultrafiltration (solid line), retentate (dash line) and permeate (dot line) for the set of operating parameter values, $TMP = 0.4$ bar and $c_r/c^* = 0.41$.

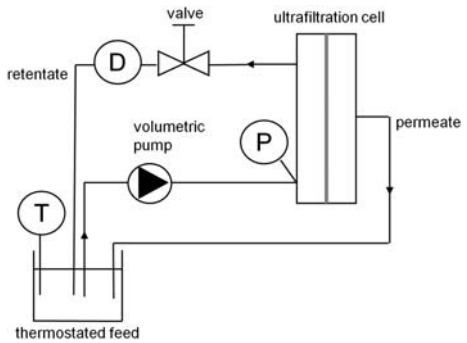

Fig. 3 Experimental device (the manometer and the flowmeter are denoted P and D, respectively).

2.3. Ultrafiltration set-up

The experimental set-up is represented in Fig. 3. It includes a Watson-Marlow 624U peristaltic pump, which pumps the PEO solution from the feed tank to the ultrafiltration module (Rayflow®2 × 100, Orelis-Novasep Group). The volume of PEO solution used for an ultrafiltration test is approximately 500 mL. The feed tank is kept at a constant temperature of 25.0 ± 0.1 °C using an RM6 Lauda cryostat. The membrane feed vein is a channel with length $L_c = 170$ mm, width 76 mm and thickness 0.5 mm. The equivalent hydraulic diameter of the channel is equal to $d_e = 1$ mm. The active surface of the membrane is equal to 129.2 cm^2 (only one membrane is mounted at a time). Transmembrane pressure (TMP) is adjusted thank to the pump and a valve located in the retentate loop, with the permeate exiting the module at atmospheric pressure. TMP is measured on entry to the module using an electronic manometer (MD10, Essor Français Electronique) accurate to 0.01 bar. The relative discrepancy between measured transmembrane pressure and the specification pressure is at the most 4%. This is chiefly related to the pulsations of the pump. The loss of pressure throughout the module (from entry to exit on the retentate side) is estimated at the most at 0.07 bar (assuming Poiseuille flow, while suction on the membrane tends to reduce that loss of pressure further), which represents 4%–20% of transmembrane pressure (for $TMP = 2$ bar and $TMP = 0.4$ bar, respectively). Retentate flow is measured using a turbine flowmeter (101-8T, McMillan Company). The pulsations of the pump cause oscillation in the flow, of an amplitude that remains below 4% of the specification flow. Finally, permeate flow is determined by weighing.

2.4. Experimental protocol

Every experimental trial is carried out with a new membrane. A trial is mainly comprised of two stages: measurement of the hydraulic resistance of the membrane in pure water, then ultrafiltration of the PEO solution as such. The ultrafiltration of PEO solutions is done at constant transmembrane pressure and at constant retentate flow, with total recycling (*i.e.* of both retentate and permeate) for 4 min. The examined transmembrane pressure is in the range from 0.4 to 2 bars (the maximum transmembrane pressure for using TEM_0.03 and TEM_0.05 membranes in our device is approximately 2 bars). For all PEO ultrafiltration trials, the retentate volume flow is set at 2.25 L min^{-1}, *i.e.*, an average speed of $u_0 = 1$ m s^{-1} in the feed channel: in these conditions, flow is laminar as the Reynolds number $Re = \rho_s u_0 d_e/\eta_s$ is equal to 1100 (where ρ_s is the density of the pure solvent). It should be noted that the ratio of permeate flow to retentate flow is less than 1%. In these conditions, it can reasonably be considered that PEO bulk concentration does not vary between feed and retentate. Samples of retentate and permeate are taken at $t = 4$ min and analysed by differential refractometry and SEC-MALS: refractometry gives access to the PEO concentration, whereas the SEC-MALS facility is used to check PEO integrity. Each ultrafiltration trial is carried out at least twice.

3. Results and discussion

The output data from the ultrafiltration experiments are mainly permeate flux (J_v, ratio of permeate volume flow to active surface of membrane) and observed rejection coefficient (R_{obs}). The input parameters examined are transmembrane pressure (TMP), PEO concentration of feed (c_r) and average steric hindrance of PEO in membrane pores (λ): $TMP = 0.4$, 0.8, 1.2 and 2 bar; $c_r =$ 0.05, 0.1, 0.2, and 0.3 g L^{-1}, *i.e.* $c_r/c^* = 0.07$, 0.14, 0.28 and 0.41 (where $c^* = 0.7$ g L^{-1} is the overlap concentration estimated in assuming that the pervaded volume of the polymer chain is a sphere of radius r_g) and λ = 1.2 and 1.8 (corresponding to membrane model TEM_0.05 and TEM_0.03, respectively).

First, we examine the effect of transmembrane pressure and PEO concentration on permeate flux and, second, the effect of permeate flux on observed rejection coefficient. Then, we determine the bulk mass transfer coefficient of the PEO chains as a function of permeate flux and we deduce the value of the true rejection coefficient. Finally, we analyse the variations in true rejection coefficient against the solvent flow rate per pore, using (i) Daoudi and Brochard's affine stretching model, (ii) de Gennes' "suction model". In particular, we quantify the effect of pore polydispersity on the shape of the forced permeation transition.

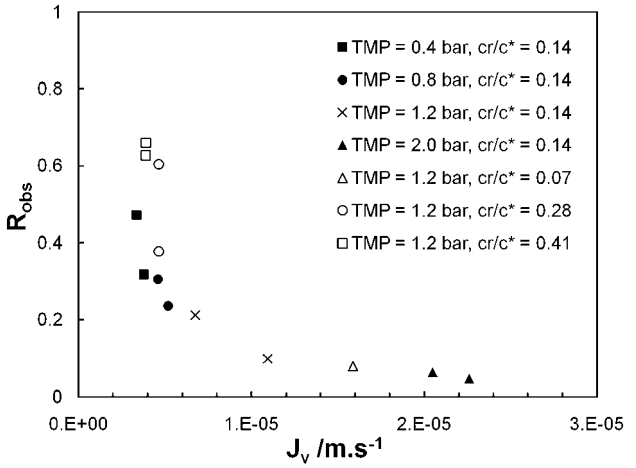

Fig. 4 Observed rejection coefficient (R_{obs}) at $t = 4$ min against instantaneous permeate flux (J_v) at $t = 4$ min for ultrafiltration tests performed with membrane model TEM_0.05 ($\lambda = 1.2$) at sets of operating parameters ($TMP = 0.4$, 0.8, 1.2, 2.0 bar; $c_r/c^* = 0.14$) and ($TMP = 1.2$ bar; $c_r/c^* = 0.07$, 0.14, 0.28, 0.41).

3.1. Permeate flux and observed rejection coefficient

Fig. 4 summarises the values of the permeate flux and observed rejection coefficient measured at $t = 4$ min for different sets of operating parameter values, *i.e.* *TMP* and c_r/c^* sets, in the case of membrane model TEM_0.05.

First, it is observed that permeate flux depends of course on the transmembrane pressure (J_v increases from 3.4×10^{-6} to 2.0×10^{-5} m s^{-1} when *TMP* varies from 0.4 to 2 bars, the PEO concentration of the feed being set at $c_r/c^* = 0.14$) but also on the POE concentration of the feed (J_v decreases from 1.6×10^{-5} to 3.9×10^{-6} m s^{-1} when c_r/c^* varies from 0.07 to 0.41, *TMP* being set at 1.2 bar). The decrease in permeate flux when PEO concentration increases is explained by concentration polarisation and by PEO chains clogging the pores. Indeed, these phenomena induce an increase in the total hydraulic resistance of the membrane. Hence, the hydraulic resistance associated with the concentration polarisation layer typically varies in a power-law relation to the feed concentration.[19,20] The exponent, determined experimentally,[21] here has a value of 0.33, in accordance with the data available in the literature, *i.e.* 0.42 for the ultrafiltration of dextran[19] and 0.3 for the ultrafiltration of polyvinylpyrrolidone.[20] Last, for the same set of operating parameter values, a dispersion of permeate flux values is seen. This dispersion is related to the history effect: the time to set transmembrane pressure prior to starting the stopwatch is not strictly identical from one trial to another; in those conditions, the total hydraulic resistance of the membrane at $t = 0$ may differ.

Fig. 4 shows that the observed rejection coefficient is closely correlated to permeate flux. R_{obs} varies from 0.66 to 0.06 when J_v varies from 3.4×10^{-6} to 2.0×10^{-5} m s^{-1}. For any trial, SEC-MALS analysis (see an example of SEC-MALS analysis in Fig. 2) shows that the differential molar mass distribution of permeate, retentate and initial feed are close together (discrepancies in molar mass and gyration radius remain within the uncertainty bracket of the SEC-MALS analysis). First, we deduce that the mechanical degradation of the PEO under the effect of shearing[22] (which could be responsible for the decrease in R_{obs} when J_v increases) remains negligible in the first four minutes of ultrafiltration. Second, as the permeate and retentate have the same POE molar mass distribution, the values of observed rejection coefficient are not just due to PEO fractions with lower molar mass (hydrodynamic diameter less than pore diameter), but also to fractions with high molar mass, which, under the effect of the shearing of the fluid are stretched and can penetrate the pores. These results suggest that (i) there is forced permeation of polymer chains at high values of J_v (ii) this phenomenon also exists at low values of J_v but less markedly, and (iii) clogging of pores by long chains, *i.e.* such as $\lambda > 1$, probably prevents shorter chains, *i.e.* such as $\lambda < 1$, from going through, hence the observed lack of separation between long and short chains.

It should be noted that on top of the phenomenon of forced permeation, the phenomenon of concentration polarisation may also affect the observed rejection coefficient: polymer chains are convected from the centre of the solution to the membrane where they tend to accumulate. For a given partition coefficient (assumed as independent of J_v) of PEO chains between the inside and outside of pores, PEO concentration at the membrane surface (c_m) increases with J_v and becomes greater than the concentration of the bulk, c_r, leading to a decrease in observed rejection coefficient. Furthermore, the PEO concentration gradient between membrane and bulk causes a back-diffusion flow of PEO chains in opposition to the convective flow.

3.2. Corrected rejection coefficient

To calculate the true rejection coefficient (R), we need a model to estimate the effective polymer concentration at the membrane surface c_m ($>c_r$, mean retentate concentration). The stagnant film model[23] expresses c_m in term of the mean retentate and permeate concentrations, the permeate flux and the solute bulk mass transfer coefficient (k_m):

$$\frac{c_m - c_p}{c_r - c_p} = e^{Jv/k_m} \tag{8}$$

Eqn (8) can be rewritten as:

$$\ln\left(\frac{1}{R_{obs}} - 1\right) = \ln\left(\frac{1}{R} - 1\right) + \frac{J_v}{k_m} \tag{9}$$

The experimental data (J_v, R_{obs}) obtained for $c_r/c^* = 0.14$ and 0.41 in the case of $\lambda = 1.2$ are plotted in the form suggested by eqn (9) with the results shown in Fig. 5: both curves are roughly linear for the smallest values of J_v as well as for the largest values of J_v and the curves are strongly non linear for the intermediate values of J_v, this behaviour being attributed to the transition from large retention to full transmission of the PEO chains. This trend has already been noticed by Latulippe *et al.* for the ultrafiltration of supercoiled plasmid DNA.[24] The bulk mass transfer coefficient k_m can be estimated as the reciprocal of the curve slope. The estimates of k_m for the experiments performed at $c_r/c^* = 0.14$ and 0.41 are reported in Fig. 6. They concur well with Lévêque's boundary layer model[25] for the smallest values of J_v and with De and Bhattacharya's model[26] for larger values of J_v. Indeed, De and Bhattacharya's approach takes into account the

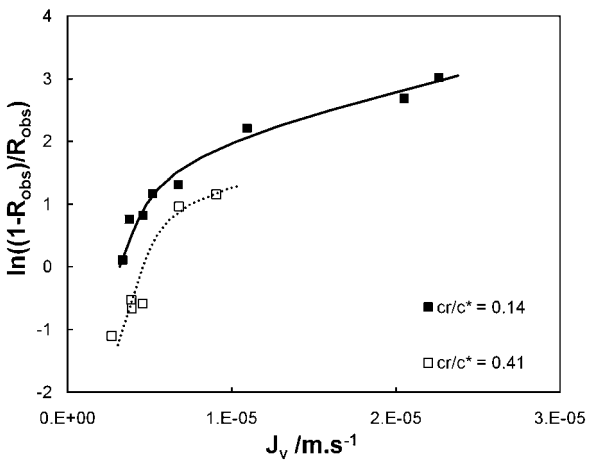

Fig. 5 Plot of $\ln(1/R_{obs} - 1)$ against the permeate flux (J_v) for ultrafiltration tests performed with membrane model TEM_0.05 ($\lambda = 1.2$) at dimensionless PEO concentration c_r/c^* equal to 0.14 and 0.41.

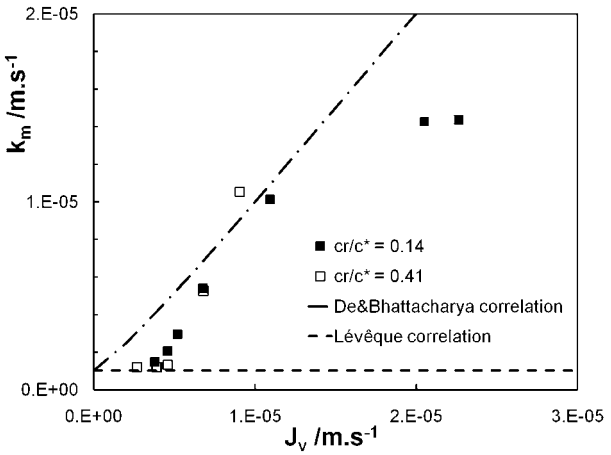

Fig. 6 Bulk mass transfer coefficient of PEO chains (k_m) against the permeate flux (J_v): experimental estimations (for $c_r/c^* = 0.14$ and 0.41) and correlations of Lévêque[25] and De and Bhattacharya.[26]

effect of suction on the developing concentration boundary layer leading to:

$$k_m = 1.85\left(\frac{\mathrm{Re}\ Sc\ d_e}{L_c}\right)^{1/3}\frac{D_\infty}{d_e}\left(1 + 0.401\alpha + 6.06\ 10^{-3}\alpha^2 - 5.96\ 10^{-5}\ \alpha^3\right) \quad (10)$$

where D_∞ is the PEO binary diffusivity in dilute free solution[18] ($D_\infty = 5.4 \times 10^{-12}$ m^2 s^{-1}, calculated with the weight-average molar mass of the PEO used in the present experiments), $Sc = \eta_s/\rho_s D_\infty$ is the Schmidt number, α is defined as $\alpha = Pe_t/(ReSc\ d_e/L_c)^{1/3}$ and $Pe_t = J_v d_e/D_\infty$ is the transverse Péclet number. It should be noted that Lévêque's model is exactly recovered from De and Bhattacharya's model in the limit of vanishing suction. Fig. 6 shows that the PEO mass transfer coefficient, k_m, is of the order of the permeate flux, J_v, which means that polarisation effects are not negligible in the present experiments.

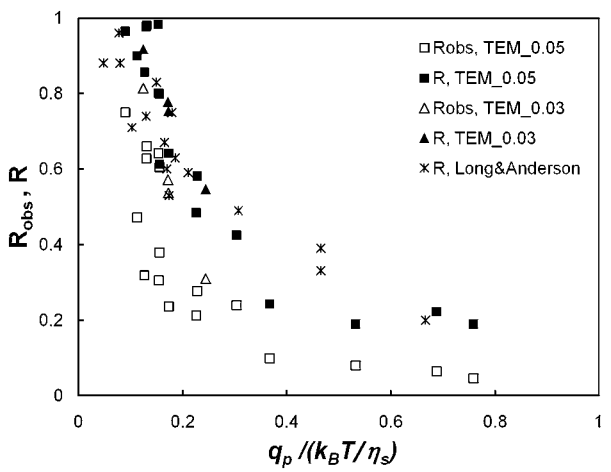

Fig. 7 The observed and the true rejection coefficients (R_{obs} and R, respectively) against the dimensionless solvent flow rate per pore ($q_p/(k_BT/\eta_s)$) for membrane models TEM_0.05 and TEM_0.03, *i.e.* $\lambda = 1.2$ and 1.8, respectively. Long and Anderson's[8] data (such as $\lambda > 1$) are also reported on the present graphic.

We plot in Fig. 7 the true rejection coefficient, R, and the observed rejection coefficient, R_{obs}, as a function of the normalized solvent flow rate per pore, $q_p/(k_BT/\eta_s)$, for $\lambda = 1.2$ and 1.8. It can be noted that the true rejection coefficient is significantly larger than the observed rejection coefficient. For the smallest value of q_p, the true rejection coefficient is close to 1 even in the case of TEM_0.05 (weight average ratio characterising hindrance, $\lambda = 1.2$). This is surprising because the fraction of PEO chains with a hydrodynamic radius smaller than the mean pore radius is estimated at about 40%. This large PEO retention is attributed to a hindrance effect[27,28] which strongly reduces polymer transmission when the polymer chains are smaller but of the order of the pore size, and to pore clogging by larger polymer chains, preventing smaller ones from passing through the membrane. For the largest values of q_p, the true rejection coefficient is significantly lower: R falls below 0.2.

The examination of the variations of R as a function of q_p shows that the transition from large retention to full transmission is gradual. This result concurs with the findings of most studies.[5,8–10] On the other hand, the examination of variations of R_{obs} alone would lead us to believe that this transition is sharp. Hence, we may expect that the sharpness of the transition observed by Jin and Wu[11] is a polarisation effect (indeed, they implicitly assimilate R_{obs} to R even though their device is not mechanically agitated).

Finally, Long and Anderson's data,[8] obtained for the ultrafiltration of polystyrene in a mixed solvent of 90% tetrachloride–10% methanol are reported in Fig. 7: it appears that Long and Anderson's data collapse into the same curve as the points representing the present experiments.

3.3. Pore polydispersity

As the pore size distribution of the membranes used in the present study has been carefully characterised, we are able to quantify the effect of the pore polydispersity on the apparent spreading of the transition. This effect could be significant (even for track-etched membranes) as the pure solvent flow rate in a pore of radius r_p scales as r_p^4. We have developed a simple "threshold model" which takes into account the pore size distribution of the membrane model (determined in section 2.1), assumes Poiseuille flow in the pores and considers that, for a given pore class, denoted i of radius r_p^i and associated frequency f_r^i, the retention of the polymer is complete (*i.e.* the true rejection coefficient of class i is equal to $R^i = 1$) when the solvent flow rate, q_p^i, in the current pore of class i is lower than q_p^c (according to Daoudi and Brochard's model). And the retention vanishes ($R^i = 0$) as soon as $q_p^i \geq q_p^c$. Then, the true rejection coefficient of the membrane expresses as:

$$R = 1 - \frac{\sum_{q_p^i \geq q_p^c} f_r^i q_p^i}{\sum_i f_r^i q_p^i} \quad (11)$$

The average solvent flow rate per pore, q_p, is given by $q_p = \sum_i f_r^i q_p^i$ and the solvent flow rate in a pore of class i reads $q_p^i = (\pi r_p^{i4}/8l\eta_s)TMP$, which can be rewritten as $q_p^i = (r_p^{i4}/\sum_i f_r^i r_p^{i4})q_p$.

Fig. 8 presents the comparison between the threshold model and the experimental values of the true rejection coefficient

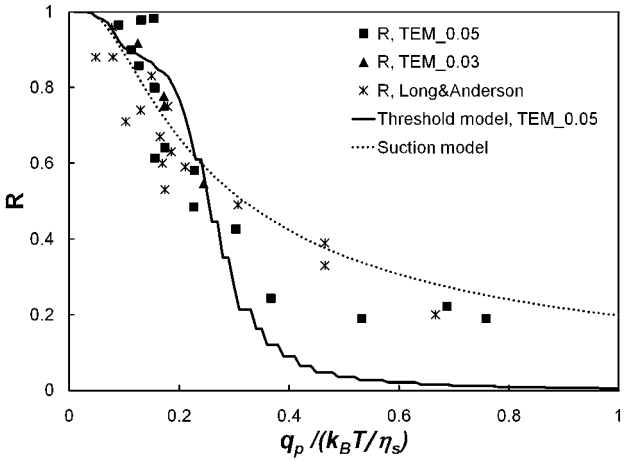

Fig. 8 Comparison between the threshold model (solid line), the suction model (dot line) and the experimental values of the true rejection coefficient (square: TEM_0.05, $\lambda = 1.2$; triangle: TEM_0.03, $\lambda = 1.8$; star: Long and Anderson's[8] data).

obtained for the membrane model TEM_0.05. The best fit is obtained for a critical solvent flow rate equal to $q_p^c = 0.27(k_BT)/\eta_s$. It should be noted that the discretisation of the pore size distribution into classes of finite width is responsible for the steps visible on the curve provided by the threshold model. Fig. 8 shows that the pore polydispersity alone cannot explain the spreading of the forced permeation transition over one decade. In particular, it fails to describe the values of the rejection coefficient for $q_p/(k_BT/\eta_s) > 0.3$. We discuss now a second model developed by de Gennes.[12]

3.4. de Gennes suction model[12]

To explain the gradual transition from large retention to full transmission, de Gennes introduced the suction model: under the flow $q_p = \pi r_p^2 u_p$ inside a pore, a polymer chain (constituted of N monomers) enters progressively. Let us consider the situation corresponding to the penetration of P ($P \leq N$) monomers. The conformation of the confined part of the chain can be pictured as a string of blobs of radius r_p. The length of this string (y) is given by:

$$y = \frac{P}{g}(2r_p) \tag{12}$$

where P/g is the number of injected blobs and g is the number of monomers per blob. g is related to r_p by $g = (2r_p/a)^{5/3}$, where a is the monomer length. The variation of the free energy of the sucked chain *versus* y is the sum of the confinement energy which opposes the chain's entry and the work of the hydrodynamic force which pushes the chain into the pore:

$$\Delta G = f_{conf}\, y - \int_0^y f_{hyd}(y)dy \tag{13}$$

The resisting force due to the confinement scales as:[29]

$$f_{conf} \approx \frac{k_BT}{r_p} \tag{14}$$

The hydrodynamic force f_{hyd} can be estimated as a Stokes drag on the blobs. Assuming that y is larger than the blob size, we get:

$$f_{hyd} \approx \frac{P}{g}\eta_s\, r_p\, u_p \tag{15}$$

The variation of free energy (13) can thus be rewritten as:

$$\Delta G \approx \frac{y}{r_p}k_BT - \eta_s\, q_p \frac{y^2}{r_p^2} \tag{16}$$

Eqn (16) indicates the existence of a barrier in free energy,

$$\Delta G^{\#} \approx \frac{(k_BT)^2}{\eta_s\, q_p} \tag{17}$$

located at

$$y^{\#} \approx \frac{k_B\, T\, r_p}{\eta_s\, q_p} \tag{18}$$

The suction of polymer chains into pores should be significant when $\Delta G^{\#}$ is at the most of the order of k_BT. The critical flux (q_p^c) corresponds to $\Delta G^{\#} \approx k_BT$ and is given by $q_p^c \approx k_BT/\eta_s$ which is identical to the critical flux provided by the affine stretching model (eqn (5)). This can be rewritten as:

$$\Delta G^{\#} = \left(\frac{q_p^c}{q_p}\right)k_BT \tag{19}$$

The energy barrier corresponds to the penetration of the first blob; as the number of sucked blobs increases, the confinement force stays constant whereas the aspiration force increases linearly with y and the chain is sucked in.

If we assume thermodynamic equilibrium between both sides of the pore entrance, the true rejection coefficient is given by:

$$R = 1 - \frac{c_p}{c_m} = 1 - \exp\left(-\frac{\Delta G^*}{k_BT}\right) = 1 - \exp\left(-\frac{q_p^c}{q_p}\right) \tag{20}$$

Then, eqn (20) can be used to fit the present experimental results together with Long and Anderson's data. The least square fit (see Fig. 8) is obtained for a critical solvent flow rate equal to $q_p^c = (0.22 \pm 0.01)k_BT/\eta_s$. When the present experimental results (resp. Long and Anderson's data) are fitted separately, the fitting value of q_p^c is equal to $q_p^c = (0.24 \pm 0.02)k_BT/\eta_s$ (resp. $q_p^c = (0.19 \pm 0.01)k_BT/\eta_s$). The discrepancy between both fitting values is attributed to supplementary interactions (physical chemical ones as opposed to purely steric and hydrodynamic ones) acting in the present experiments between the polymer chains and the membrane surface and between the polymer chains themselves.[30]

The magnitude of the critical solvent flow rate concurs with Daoudi and Brochard's[3] and de Gennes'[12] theoretical prediction. It is much larger than Jin and Wu's[11] experimental estimate, *i.e.* $q_p^c = 0.006k_BT/\eta_s$. We attribute this discrepancy to the conical shape of the pores of the special double-layer membrane used by Jin and Wu.[11] Indeed, according to Daoudi and Brochard,[3] the critical solvent flow rate in a conical pore is smaller than the critical solvent flow rate in a cylindrical pore as long as the radius of the cone entrance is larger than the polymer radius: in the limit of a small cone angle, it is given by $q_p^c \approx \varepsilon k_BT/\eta_s$ where ε is the angle of the cone.

It must be noticed that as in section 3.3, it is possible to take into account the pore size distribution of the membrane. The true rejection coefficient is then given by:

$$R = 1 - \frac{\sum_i f_r^i \exp\left(-q_p^c/q_p^i\right) q_p^i}{\sum_i f_r^i q_p^i} \quad (21)$$

For the present membrane models, *i.e.* TEM_0.05 and TEM_0.03, the pore size distribution is too narrow to significantly affect the estimation of q_p^c.

4. Conclusion

For the first time, forced permeation transition has been quantitatively analysed using de Gennes' suction model.

The comparison of the present experimental results (PEO aqueous solution through track-etched polycarbonate membrane) and those of Long and Anderson[8] (polystyrene solution through track-etched mica sheet) shows that the variations of the true rejection coefficient, R, as a function of the dimensionless solvent flow rate per pore, $q_p/(k_BT/\eta_s)$, collapse into the same curve. This curve should be universal for flexible linear polymers in good solvent (as long as $r_h > r_p$).

The transition from total retention ($R = 1$) to full transmission ($R = 0$) does not occur as abruptly as Daoudi and Brochard's[3] affine stretching model predicts. This confirms the findings of earlier experimental studies.[5,8–10] The present experiments establish that the smoothness of the transition is not due to the pore polydispersity of the membrane or to the polymer polydispersity of the feed but is intrinsic to the permeation phenomenon.

The shape of R *versus* q_p is well fitted by de Gennes'[12] suction model, based on the free energy barrier that a polymer chain must overcome to enter a pore. The equation of the rejection curve can be written as $R = 1 - \exp(-q_p^c/q_p)$. The critical solvent flow rate, q_p^c, has been estimated at $q_p^c = (0.22 \pm 0.01)k_BT/\eta_s$. It is independent upon the pore size and the polymerization index as predicted by Daoudi and Brochard[3] and de Gennes.[12]

References

1 C. K. Colton, C. N. Satterfield and C. J. Lai, *AIChE J.*, 1975, **21**, 289–298; C. N. Satterfield, C. K. Colton, B. de Turckheim and T. M. Copeland, *AIChE J.*, 1978, **24**, 937–940.
2 P. G. De Gennes, *Macromolecules*, 1976, **4**, 587–593.
3 S. Daoudi and F. Brochard, *Macromolecules*, 1978, **11**, 751–758.
4 D. S. Cannell and F. Rondelez, *Macromolecules*, 1980, **13**, 1599–1602.
5 Q. T. Nguyen and J. Neel, *J. Membr. Sci.*, 1983, **14**, 111–128.
6 T. D. Long and J. L. Anderson, *J. Polym. Sci., Polym. Phys. Ed.*, 1985, **23**, 191–197.
7 G. Guillot, L. Léger and F. Rondelez, *Macromolecules*, 1985, **18**, 2531–2537.
8 T. D. Long and J. L. Anderson, *J. Polym. Sci., Polym. Phys. Ed.*, 1984, **22**, 1261–1281.
9 G. Guillot, Ph. D. Thesis, University of Paris Sud, 1986.
10 M. A. M. Beerlage, M. L. Heijnen, M. H. V. Mulder, C. A. Smolders and H. Strathmann, *J. Membr. Sci.*, 1996, **113**, 259–273.
11 F. Jin and C. Wu, *Phys. Rev. Lett.*, 2006, **96**, 237801–4.
12 C. Gay, P.-G. de Gennes, E. Raphaël and F. Brochard-Wyart, *Macromolecules*, 1996, **29**, 8379–8382; P.-G. De Gennes, in *Advances in Polymer Science*, ed. S. Granick, Springer, Berlin, 1999, vol. 138, pp. 92–105; T. Sakaue, E. Raphaël, P.-G. de Gennes and F. Brochard-Wyart, *Europhys. Lett.*, 2005, **72**(1), 83–88.
13 A. P. Markesteijn, O. B. Usta, I. Ali, A. C. Balazs and J. M. Yeomans, *Soft Matter*, 2009, **5**, 4575–4579.
14 J. I. Calvo, A. Hernandez, G. Caruana and L. Martinez, *J. Colloid Interface Sci.*, 1995, **175**, 138–150.
15 C. Schonenberger, B. M. I. vanderZande, L. G. J. Fokkink, M. Henny, C. Schmid, M. Kruger, A. Bachtold, R. Huber, H. Birk and U. Staufer, *J. Phys. Chem. B*, 1997, **101**, 5497–5505; P. Y. Apel, I. V. Blonskaya, S. N. Dmitriev, O. L. Orelovitch and B. Sartowska, *J. Membr. Sci.*, 2006, **282**, 393–400.
16 S. Paillet, B. Grassl and J. Desbrieres, *Anal. Chim. Acta*, 2009, **636**(2), 236–41.
17 G. Dupuis, J. Rigolini, G. Clisson, D. Rousseau, R. Tabary and B. Grassl, *Anal. Chem.*, 2009, **81**(21), 8993–9001.
18 K. Devanand and J. C. Selser, *Macromolecules*, 1991, **24**, 5943–5947.
19 H. M. Yeh and T. W. Cheng, *Sep. Sci. Technol.*, 1993, **28**, 1341–1355.
20 H. M. Yeh and H. H. Wu, *J. Membr. Sci.*, 1997, **124**, 93–105.
21 L. Béguin, Ph. D. Thesis, Ecole Centrale Paris, 2008.
22 S. A. Vanapalli, M. T. Islam and M. J. Solomon, *Phys. Fluids*, 2005, **17**, 095108; A. R. D'Almeida and M. L. Dias, *Polym. Degrad. Stab.*, 1997, **56**, 331–337; B. A. Buchholz, J. M. Zahn, M. Kenward, G. W. Slater and A. E. Barron, *Polymer*, 2004, **45**, 1223–1234.
23 L. J. Zeman, A. L. Zydney, in *Microfiltration and Ultrafiltration, Principles and Applications*, ed. Marcel Dekker, Inc., New York, 1996, ch. 7, pp. 354–357.
24 D. R. Latulippe, A. Kimberlyn and A. L. Zydney, *J. Membr. Sci.*, 2007, **294**, 169–177.
25 M. A. Lévêque, *Ann. Mines Paris*, 1928, **13**, 201–409.
26 S. De and P. K. Bhattacharya, *J. Membr. Sci.*, 1997, **128**, 119–131.
27 J. D. Ferry, *J. Gen. Physiol.*, 1936, **20**(1), 95–104.
28 P. Dechadilok and W. M. Deen, *Ind. Eng. Chem. Res.*, 2006, **45**, 6953–6959.
29 M. Daoud and P.-G. de Gennes, *J. Phys.*, 1977, **38**(1), 85–93.
30 P. Pang and P. Englezos, *Fluid Phase Equilib.*, 2002, **194–197**, 1059–1066; M. W. Liberatore and A. J. McHugh, *J. Non-Newtonian Fluid Mech.*, 2005, **132**, 45–52.